Microelectronic Engineering 112 (2013) 188–192

Contents lists available at SciVerse ScienceDirect

Microelectronic Engineering

journal homepage: www.elsevier.com/locate/mee

Simulation study of an electrically read- and writable magnetic logic gate

Thomas Windbacher *, Oliver Triebl, Dmitry Osintsev, Alexander Makarov, Viktor Sverdlov, Siegfried Selberherr

Institute for Microelectronics, TU Wien, Gußhausstraße 27-29, A-1040 Vienna, Austria

ARTICLE INFO

Article history:
Available online 29 January 2013

Keywords:
Anisotropic magneto resistance
Magnetic logic gate
Constriction
(*Ga*, *Mn*)*As*
Metal insulator transition

ABSTRACT

In order to keep up with economic growth and competitiveness the performance of microelectronic components will continuously increase, thanks to the introduction of new device types and materials. Spin based technologies are promising candidates because of their fast switching capability, high endurance, and non-volatility. Furthermore, the use of spin as a degree of freedom permits the combination of information storage and processing in a single device creating a fully non-volatile information processing system and thus allowing an even denser layout of simplified building blocks. Recently a fully electrical read–write 1 bit demonstrator memory device out of a ferromagnetic semiconductor has been shown and it has been proposed to extend this device to a logic XOR gate. However, up to now neither the feasibility of this gate nor the extendability to further logic gates has been shown. In this work we carried out a rigorous simulation study of the proposed logic gate. We are able to show that firstly the magnetization can be switched diagonally. Secondly, by changing the relative angle between the current flow path and the magnetization, not only a XOR gate is feasible but also (N)AND and (N)OR gates can be realized.

1. Introduction

Diluted magnetic semiconductors (DMS) belong to the group of extensively studied (prototype) materials for future devices [1]. Especially one member of this group – (*Ga*, *Mn*)*As* – is of interest due to its compatibility with established semiconductor technology, carrier mediated ferromagnetism caused by *sp*—*d* exchange [2], and its cubic anisotropy which can be modified to an in-plane bi-axial anisotropy ([100], [010]) for compressively strained thin films or an easy axis out of plane ([001]) for tensile strained thin films [3]. Hümpfner et al. [4] showed that by lithographical means local stress relaxation can be used to taylor the local anisotropy type. It was demonstrated that due to anisotropic stress relaxation, leads along [100] and [010] exhibit uni-axial anisotropies along these axes, respectively. Mark et al. [5] connected two pairs of such leads (along [100] and [010]) with a disk exhibiting a bi-axial anisotropy and thus enabled a realization of an electrically writable 1 bit demonstrator device. They also proposed an electrically read- and writable XOR gate consisting of two disks connected by a small constriction. Pappert et al. [6] connected two orthogonal and uni-axially relaxed leads by a small constriction and showed that the overall electrical resistance of the structure depends on the angle between the current flow $\vec{j}$ and the local magnetization $\vec{m}$ at the constriction. For a small constriction (~tens of nanometers) and $\vec{j} \| \vec{m}$ the structure exhibited a several times bigger resistance (up to more than 5 times) compared to $\vec{j} \perp \vec{m}$. Therefore, combining two disks with bi-axial anisotropies, uni-axial leads, and a constriction connecting the disks, allows to combine memory and logic in one structure. Additionally this device allows an even denser layout on top of the density gain by scaling due to the merging of logic and memory units. We show that the disks can be switched by horizontal and diagonal current flow, scaling leads to smaller switching times, and the possibility of further logic gates by changing the angle between the current density $\vec{j}$ and the magnetization $\vec{m}$ at the constriction.

2. Methods

For the simulation study of the proposed structure disk radii of 160, 80, and 40 nm were used. Furthermore, a fixed constriction length and width of 15 nm, a saturation magnetization M_S of 32000 A/m [2], a cubic anisotropy with its easy axis oriented parallel to the leads and a cubic anisotropy constant K_C of 2000 J/m^3 [3] for the (*Ga*, *Mn*)*As* film were assumed. It was further supposed

* Corresponding author. Tel.: +43 58801/36018; fax: +43 58801/36099.
E-mail addresses: Windbacher@iue.tuwien.ac.at (T. Windbacher), Triebl@iue.tuwien.ac.at (O. Triebl), Osintsev@iue.tuwien.ac.at (D. Osintsev), Makarov@iue.tuwien.ac.at (A. Makarov), Sverdlov@iue.tuwien.ac.at (V. Sverdlov), Selberherr@iue.tuwien.ac.at (S. Selberherr).

0167-9317/$ - see front matter © 2013 Elsevier B.V. All rights reserved.
http://dx.doi.org/10.1016/j.mee.2012.12.030

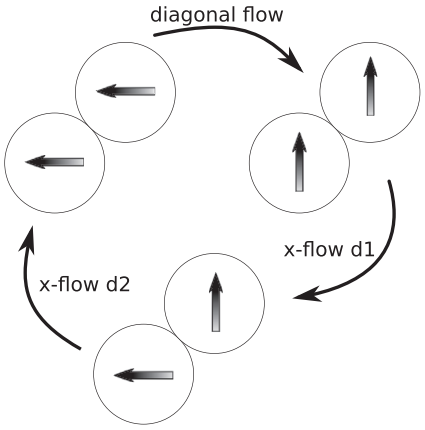

Fig. 1. The different initial and ending states and the current paths needed for transition between these states are depicted. The cycle begins with both disks exhibiting a magnetization along 90° and applying a horizontal current flow through disk $d1$ to reach the state, where the magnetization in $d1$ is flipped to 180°, while in disk $d2$ the magnetization is still oriented along 90° (x-flow $d1$). From there a horizontal current flow is applied through $d2$ to orient the disk in the same direction as $d1$ (x-flow $d2$). In order to reset the two disks to their initial state a diagonally flowing and through the constriction passing current is applied (diagonal flow).

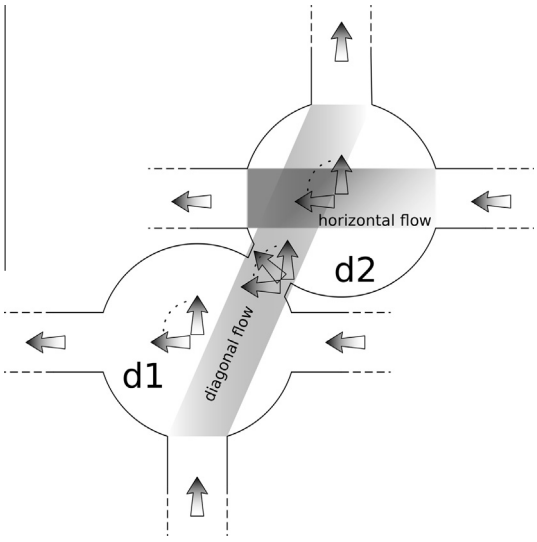

Fig. 2. The magnetization in the leads is fixed and oriented along 180° for horizontal leads and along 90° for vertical leads. The disks can be switched between the two states by either applying a horizontal or a diagonal current. At the constriction the resulting magnetization is a superposition of the magnetizations in $d1$ and $d2$ and, therefore, the magnetization at the constriction is switched in multiples of 45° between 90° and 180°.

that the magnetization of the leads is fixed, Gilbert damping $\alpha = 0.02$, current polarization $P = 0.7$, a dimensionless parameter $\beta = \alpha$ for the non-adiabatic spin-transfer torque (STT) contribution [7], and a uniform exchange constant A_{exch} of 4×10^{-14} J/m [8]. In a first step current density profiles for the different radii and current paths from self-consistent transport simulations [9] were gained (see Figs. 6–8). These profiles were used in a STT model, which was extended to enable arbitrary 2D current density profiles. The model is based on a STT model from IBM research Zürich [10] and takes advantage of an Object Oriented Micromagnetic Framework [11]. Current densities between 1×10^{10} and 5×10^{11} A/m^2 and a pulse time of 20 ns were used.

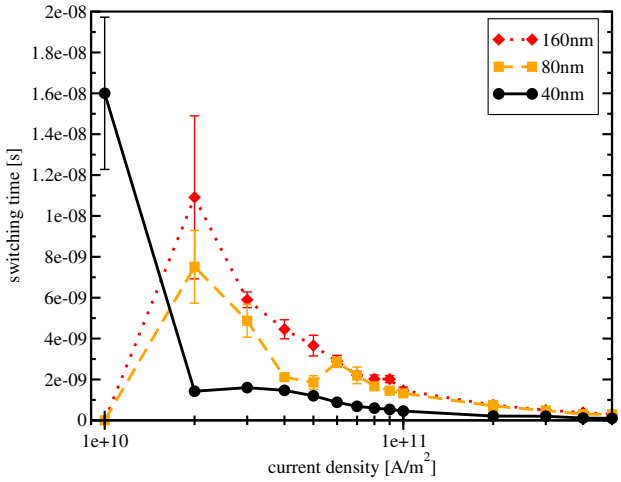

Fig. 3. Switching times for x-flow $d1$ at 40, 80, and 160 nm, respectively.

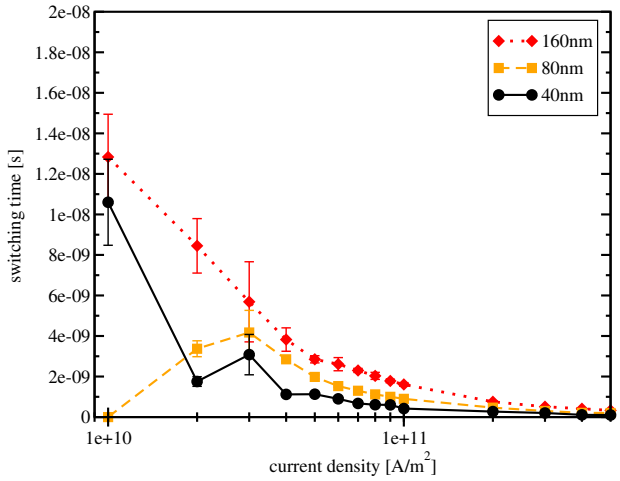

Fig. 4. Switching times for x-flow $d2$ at 40, 80, and 160 nm, respectively.

Out of all possible switching combinations a representative path that switches between three different logic states was studied (see Fig. 1), taking care that every disk is at least switched once and at the end of the cycle the initial state is regained. Switching is realized by either switching a single disk with a horizontal current flow (x-flow $d1/d2$) or by a diagonal current flowing through the constriction (cf. Figs. 2,6,7,8).

3. Results

3.1. Switching times

In order to get a relation between the switching times, applied current densities, and scaling, the switching times as function of applied current density and disk size were extracted. The switching time has been defined as the difference between the start of the current pulse and when the magnetization reaches 80% of its equilibrium state (for a successful switching). Furthermore, to improve the accuracy of the results, all data points shown are an average over several simulations (in the range of ±5% of the corresponding current density) and the error bars depicted in Figs. 3–5 state the respective standard deviation $\pm\sigma$. In cases without switching events the corresponding switching times were set to 0 s. The switching probabilities (number of successful outcomes over all simulations) are in the range of $\approx 30\%$ to $\approx 90\%$ and a total aver-

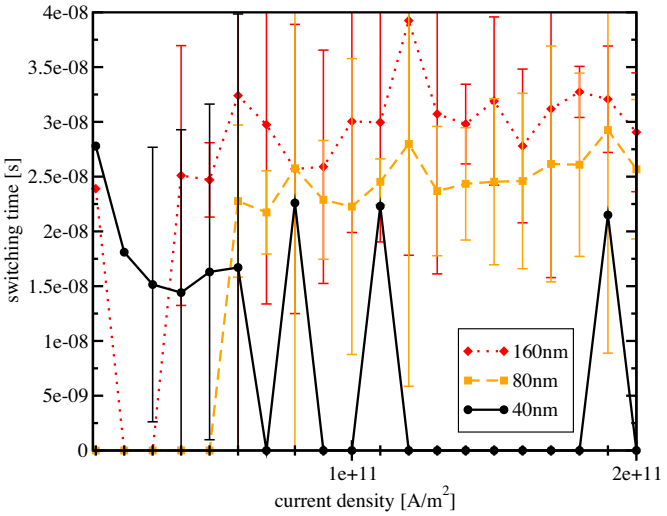

Fig. 5. Switching times for diagonal flow at 40, 80, and 160 nm, respectively.

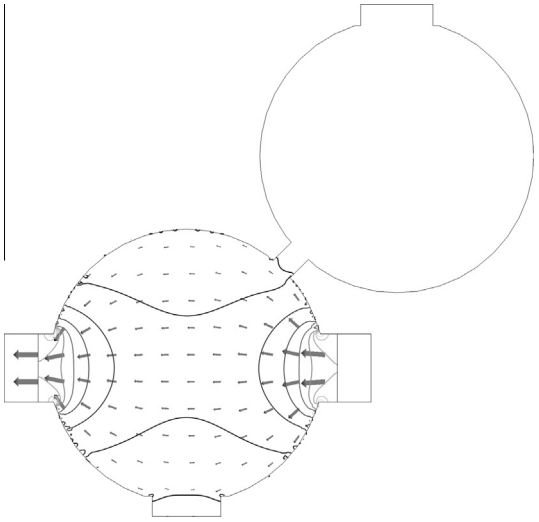

Fig. 7. Current density profile for x-flow $d1$ and a disk radius of 80 nm.

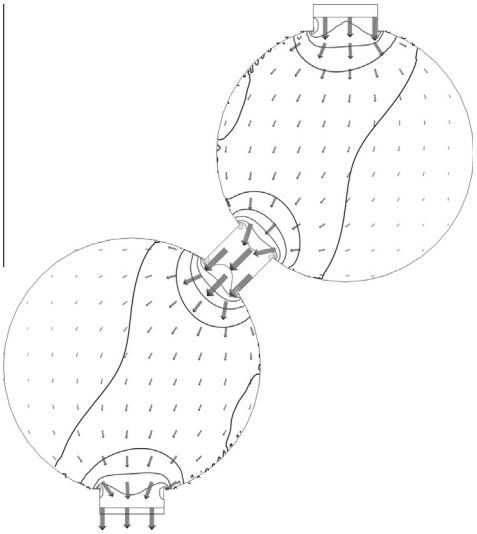

Fig. 6. Current density profile for diagonal flow and a disk radius of 40 nm.

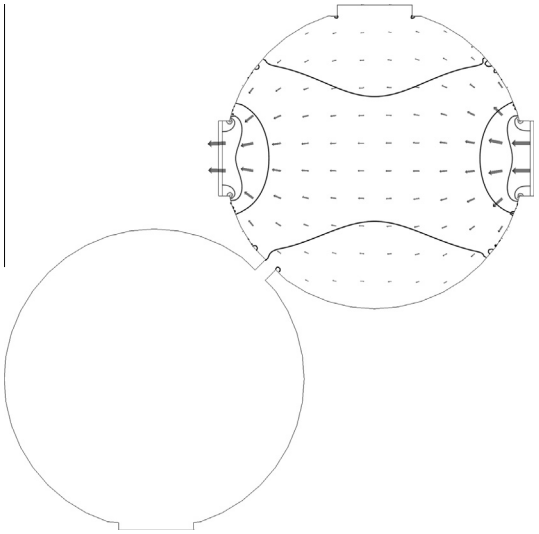

Fig. 8. Current density profile for x-flow $d2$ and a disk radius of 160 nm.

age of 75.5% for x-flow $d1$; $\approx$ 20% to 100% and a total average of 97.5% for x-flow $d2$; and $\approx$ 10% to $\approx$ 80% and a total average of 41.8% for diagonal flow, respectively.

First of all one can see that smaller disks exhibit faster switching times and that successful switching starts at $\approx 10^{10}$ A/m^2 in conjunction with large error bars and small switching probabilities. Looking at the corresponding switching probabilities shows that switching $d2$ with a horizontal flow is more probable than switching $d1$ via a horizontal flow. This is related to the energy states before and after switching. In the case of x-flow $d1$ (see Fig. 1) the initial state with both disks oriented along 90° is lower in energy compared to the ending state where $d1$ points along 180° and $d2$ along 90°. Therefore, the system tends to slip back into its initial state, while for x-flow $d2$ the ending state is lower in energy compared to its initial state, which leads to a preferred relaxation into the ending state. This can also be seen in Fig. 5, where the initial state is also lower in energy compared to its ending state and the constriction further impedes pushing the desired magnetization orientation into the second disk. The difference in the onset of the switching current densities between the 40, 80, and 160 nm in Fig. 5 can be explained by the difference in local spin torques due to the local current densities which are higher for 40 nm compared to the 80 nm/160 nm. Due to the obstruction at the constriction a larger amount of disturbances, e.g. vortices, domain walls, etc., is injected into the second disk, which leads to a longer relaxation and thus longer switching time compared to the horizontal switching paths.

It was also observed that during the pulse often only the first disk $d1$ flipped, while the second disk $d2$ could not be switched due to the domain wall pinning at the constriction. Hence, in order to reset the structure, instead of one pulse, two subsequent pulses with opposite polarity are able to switch both disks, since the constriction protects the respective other disk from being flipped. Alternatively it may be faster to apply only one pulse but change the current flow path in a way that the current will flow from the top/bottom contacts to the corresponding right and left contacts in the disks, thus avoiding to pass the constriction. However, these alternatives have to be thoroughly investigated in further studies.

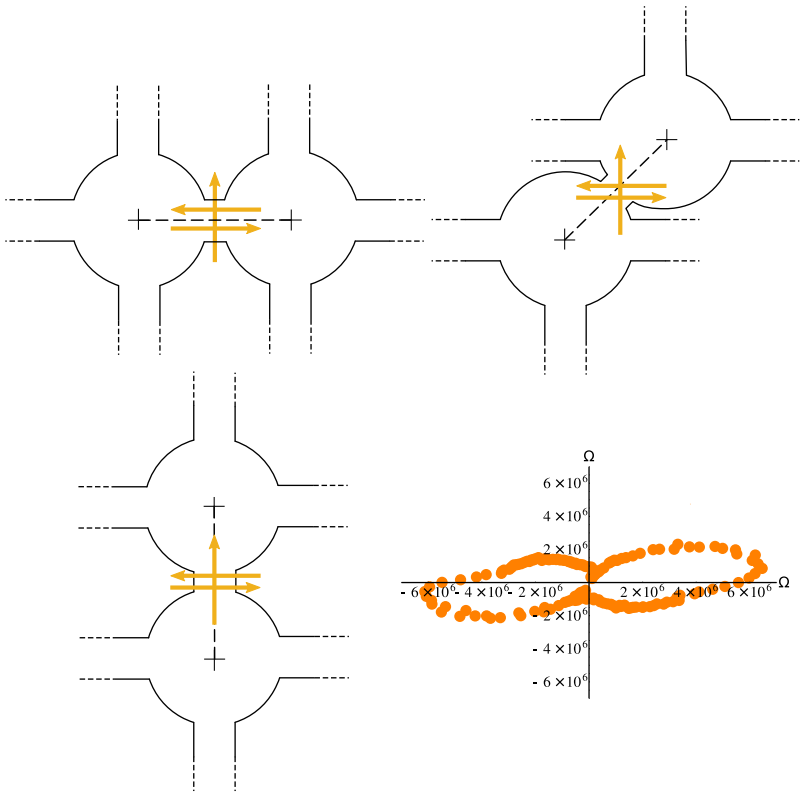

Fig. 9. Three different constriction angles (0°, 45°, and 90°) have been studied. The dashed lines show the current flow path, while the arrows denote the different magnetization orientations for operation (0°/90° and 90°/180°). The polar plot depicts the constriction resistance as a function of relative angle $\Delta\varphi$ between current density $\vec{j}$ and magnetization $\vec{m}$ at the constriction [6].

Additionally one should mention, that in the region where the disks are connected to the contacts the local current density is non-uniform; the divergent orientation of the current density in these regions, promotes the formation of disturbances like cortices, which are subsequently pushed through the disk where they relax after some time. Therefore, optimizing the current density and orientation in the contact region can be used to reduce the formation of disturbances to further accelerate switching.

3.2. Available logic gate types

Since the overall electrical resistance of the device structure is dominated by the resistance contribution of the constriction, due to its small cross section compared to the cross sections of the disks, a change in the constriction resistance can be exploited for sensing logic states. This change is accomplished by an anisotropic magneto resistance effect in $(Ga, Mn)As$ and depends on the relative angle between current density and magnetization [6]. Simulations were carried out to clarify the current orientation in the constriction (see Fig. 6) and it was found that for this set up the current is parallel to the constriction walls. Therefore, tuning the device characteristics is only possible by changing the orientation of the cubic anisotropy axis, e.g. by rotating the layout of the device, the constriction of the disks with respect to each other, and/or choosing different magnetization orientations for operation.

Three angles $\varphi = 0°, 45°$, and 90° with the easy axes fixed along [1 0 0] and [0 1 0] as well as two magnetization orientations for operation (0°/90° and 90°/180°) have been studied (see Fig. 9).

As mentioned before the current flows parallel to the constriction with constriction angle φ, while the magnetization $\vec{m}$ at the constriction is a superposition of the magnetizations of the disks $d1$ and $d2$. For instance, when $d1$ and $d2$ are oriented along 90° the magnetization $\vec{m}$ at the constriction will also point along 90°. If in this case the constriction is oriented along 0° (see Fig. 9) the current will also flow along 0°, which results in a relative angle $\Delta\varphi = 90°$. Comparing this angle with the polar plot in Fig. 9 points to a low resistance state. While for $\varphi = 0°$ and $d1 = d2 = 180°$ $\Delta\varphi = 180°$ points to a high resistance state. In this manner the resistance states for all possible magnetization combinations can be determined.

Thus, for $\varphi = 0°$ (both disks line up along [1 0 0]) and 90°/180° the device exhibits AND gate characteristics, while for 0°/90° it shows a NOR gate behavior. At $\varphi = 45°$ (both disks line up along [1 1 0]) and 90°/180° the device only exhibits low resistance states, while for 0°/90° a XOR gate is available. If $\varphi = 90°$ (both disks line up along [0 1 0]) the available logic gates are NOR and AND for 90°/180° and 0°/90°, respectively, which is also consistent with geometrical symmetry considerations.

4. Conclusion

It was found that the device can be switched by a horizontal current flow path as well as a diagonal current passing through the constriction. However, due to the differences in starting and ending energies as well as the pinning of the magnetization at the constriction, a horizontal flow path is more reliable ($\approx 30\%$ to $\approx 90\%$ and a total average of 75.5% for x-flow $d1$; $\approx 20\%$ to 100% and a total average of 97.5% for x-flow $d2$; and $\approx 10\%$ to $\approx 80\%$ and a total average of 41.8% for diagonal flow) and faster (x-flow $d1 : \approx 16$ ns to ≈ 100 ps; x-flow $d2 : \approx 13$ ns to ≈ 100 ps; d-flow: ≈ 40 ns to ≈ 15 ns).

Furthermore, one can engineer different kinds of logic gates by changing the relative position of the disks, rotating the layout or the crystal orientation, and/or utilizing different magnetization

orientations for operation. Since by this approach (N)AND, (N)OR, and XOR gates are available, basic building blocks for arbitrary complex logic functions are at hand and open the possibility of non-volatile information processing.

Acknowledgement

This research is supported by the European Research Council through the Grant #247056 MOSILSPIN.

References

[1] T. Dietl, Diluted Ferromagnetic Semiconductors – Theoretical Aspects, John Wiley & Sons, Ltd., 2007. http://dx.doi.org/10.1002/9780470022184.hmm533.
[2] H. Ohno, A. Shen, F. Matsukura, A. Oiwa, A. Endo, S. Katsumoto, Y. Iye, Appl. Phys. Lett. 69 (3) (1996) 363–365, http://dx.doi.org/10.1063/1.118061.
[3] M. Abolfath, T. Jungwirth, J. Brum, A.H. MacDonald, Phys. Rev. B 63 (2001) 054418, http://dx.doi.org/10.1103/PhysRevB.63.054418.
[4] S. Hümpfner, K. Pappert, J. Wenisch, K. Brunner, C. Gould, G. Schmidt, L. Molenkamp, M. Sawicki, T. Dietl, Appl. Phys. Lett. 90 (10) (2007) 102102, http://dx.doi.org/10.1063/1.2710478.
[5] S. Mark, P. Dürrenfeld, K. Pappert, L. Ebel, K. Brunner, C. Gould, L.W. Molenkamp, Phys. Rev. Lett. 106 (2011) 057204, http://dx.doi.org/10.1103/PhysRevLett.106.057204.
[6] K. Pappert, S. Hümpfner, C. Gould, J. Wenisch, K. Brunner, G. Schmidt, L. Molenkamp, Nat. Phys. 3 (8) (2007) 573–578, http://dx.doi.org/10.1038/nphys652.
[7] J. Curiale, A. Lemaître, C. Ulysse, G. Faini, V. Jeudy, Phys. Rev. Lett. 108 (2012) 076604, http://dx.doi.org/10.1103/PhysRevLett.108.076604.
[8] C. Gourdon, A. Dourlat, V. Jeudy, K. Khazen, H.J. von Bardeleben, L. Thevenard, A. Lemaître, Phys. Rev. B 76 (2007) 241301, http://dx.doi.org/10.1103/PhysRevB.76.241301.
[9] Institute for Microelectronics, TU Wien, Gußhausstraße 27-29, 1040 Wien, Austria/Europe, Minimos-NT Device and Circuit Simulator Release 2.1. Available from: <http://www.iue.tuwien.ac.at/software/minimosnt>.
[10] A. Vanhaverbeke, OOMMF Extension for Current-Induced Domain Wall Motion, January 2008. Available from: <http://www.zurich.ibm.com/st/magnetism/spintevolve.html>.
[11] M. Donahue, D. Porter, OOMMF User's Guide, Interagency Report NISTIR 6376, version 1.0.